NLRP3 inflammasome activation in cigarette smoke priming for *Pseudomonas aeruginosa*-induced acute lung injury☆

Alexis White [a], Zhengke Wang [a], Xing Wang [a], Michelle King [a], Cynthia Guo [a], Chris Mantsounga [a], Alfred Ayala [c], Alan R. Morrison [a,b], Gaurav Choudhary [a,b], Frank Sellke [d], Eboni Chambers [a], Lorraine B. Ware [e], Sharon Rounds [a,b], Qing Lu [a,b,*,1]

[a] *Vascular Research Laboratory, Providence Veterans Affairs Medical Center, Providence, RI, USA*
[b] *Department of Medicine, The Warren Alpert Medical School of Brown University, Providence, RI, USA*
[c] *Department of Surgery, The Warren Alpert Medical School of Brown University and Lifespan-Rhode Island Hospital, Providence, RI, USA*
[d] *Cardiothoracic Surgery, The Warren Alpert Medical School of Brown University and Lifespan-Rhode Island Hospital, Providence, RI, USA*
[e] *Division of Allergy, Pulmonary, and Critical Care Medicine, Department of Medicine, Vanderbilt University School of Medicine, Nashville, TN, USA*

ARTICLE INFO

ABSTRACT

It is increasingly recognized that cigarette smoke (CS) exposure increases the incidence and severity of acute respiratory distress syndrome (ARDS) in critical ill humans and animals. However, the mechanism(s) is not well understood. This study aims to investigate mechanism underlying the priming effect of CS on *Pseudomonas aeruginosa*-triggered acute lung injury, by using pre-clinic animal models and genetically modified mice. We demonstrated that CS impaired *P. aeruginosa*-induced mitophagy flux, promoted p62 accumulation, and exacerbated *P. aeruginosa*-triggered mitochondrial damage and NLRP3 inflammasome activation in alveolar macrophages; an effect associated with increased acute lung injury and mortality. Pharmacological inhibition of caspase-1, a component of inflammasome, attenuated CS primed *P. aeruginosa*-triggered acute lung injury and improved animal survival. Global or myeloid-specific knockout of IL-1β, a downstream component of inflammasome activation, also attenuated CS primed *P. aeruginosa*-triggered acute lung injury. Our results suggest that NLRP3 inflammasome activation is an important mechanism for CS primed *P. aeruginosa*-triggered acute lung injury. (total words: 155).

1. Introduction

Over one billion of the world's population [1], including 18.5% of Americans [2], are active tobacco smokers. It is well known that smokers are more susceptible to respiratory infections [3,4] and have increased risk for pneumonia following bacterial and viral infections [5,6]. Community-acquired pneumonia is common among smokers [7]. A growing body of epidemiologic evidence indicates that smokers also have increased risk for acute respiratory distress syndrome (ARDS) following severe blunt trauma [8], sepsis [9], surgery [10,11], blood transfusions [12], or lung transplantation [13]. Coinciding with

smoking cessation, the incidence of ARDS has significantly decreased in past decades in US [14]. Cigarette smoking also prolongs the duration of intensive care unit stays and increases mortality in critically ill patients [15]. Smokers surviving ARDS often have a poorer health-related quality of life compared to non-smokers [16]. Despite great improvements in supportive care, ARDS continues to have unacceptably high mortality (30–40%) and long-term morbidity [14], due to lack of specific drug therapy and heterogeneity of causes and risk factors of the syndrome. ARDS caused by SARS-Cov-2 virus has underscored the urgent need to develop novel adjuvant therapies to combat this devastating syndrome. A recent study of the Cleveland Clinic COVID-19

Registry indicated a dose-response association between pack-years of smoking and increased hospitalization and mortality [17]. It remains unclear why smokers develop ARDS more often and with greater mortality than non-smokers. In order to develop targeted effective therapies for ARDS patients with a history of smoking, it is important to understand the underlying mechanism(s) of cigarette smoke (CS) priming for ARDS.

Pneumonia, one of the top ten leading causes of death in the United States [18], causes 35–50% of ARDS cases [19]. *Pseudomonas aeruginosa* (*P. aeruginosa*), a gram-negative opportunistic pathogen, remains a public health threat partially due to emerging multidrug-resistance [20]. *P. aeruginosa* rarely infects healthy humans, but often causes ventilator- and health care-associated pneumonia and lung infections in cystic fibrosis, immunodeficiency, and COPD [20]. Human smokers have exacerbated lung injury after inhalation of lipopolysaccharide (LPS), a membrane component of *P. aeruginosa* and other Gram negative pathogens [21]. We have previously shown that CS exacerbates LPS-induced acute lung injury (ALI) in mice [22–24]. In this study, we tested the effect of CS on *P. aeruginosa*-induced ARDS.

The inflammasome, a multimeric protein platform, is central to innate immunity and inflammation [25]. Nucleotide-binding oligomerization domain, leucine-rich repeat and pyrin domain-containing protein 3 (NLRP3) inflammasome is a member of the Nod-like receptor (NLR) inflammasome family. The NLRP3 inflammasome is composed of NLRP3, which interacts with an adaptor protein, apoptosis-associated speck-like protein containing a caspase-recruitment domain (ASC) and pro-caspase-1, leading to self-cleavage (activation) of caspase-1, which subsequently causes maturation and release of IL-1β and IL-18, and ultimately pyroptosis (caspase 1-dependent inflammatory cell death). Mitophagy (mitochondrial autophagy), a process of eliminating damaged or unwanted mitochondria, is essential for mitochondrial homeostasis [26]. Mitophagy is initiated by Parkin (an E3 ubiquitin ligase) and PINK1 (PTEN-induced kinase 1) and sequenced by recruitment of mitophagy proteins including p62 and microtubule-associated protein light chain 3 (LC3) to form autophagosomes, which subsequently fuse with lysosomes to form autolysosomes, where the damaged mitochondria and associated proteins are degraded [27]. The process of autophagosome-lysosome fusion and degradation of the cargo is termed as mitophagy flux. Whether NLRP3 inflammasome and mitophagy are involved in CS primed ARDS is unknown and investigated in this study.

2. Materials & methods

Reagents: Antibodies directed against pro-caspase-1, p20-caspase-1, SQSTM1 (p62), Parkin, PINK1, Beclin-1, and β-actin were purchased from Santa Cruz Biotechnology (Santa Cruz, CA). Antibodies directed against NLRP3 and ASC were from Adipogen (San Diego, CA). Antibodies directed against phospho-MLKL (Thr357/Ser358), HMGB1, LC-3B, and caspase-3 were purchased from Cell Signaling Technologies (Danvers, MA). Anti-IL-1β antibody and ELISA kits for KC, MIP2, and IL10 were purchased from R&D Systems (Minneapolis, MN). ELISA kits for TNF-α and IL-6 were purchased from BD (Franklin Lakes, NJ). Anti-CD68 antibody was purchased from Abcam (Cambridge, UK) and anti-Von Willebrand factor (vWF) antibody was purchased from DAKO (Carpinteria, CA). Prolong Gold anti-fade reagent with DAPI was from Life Technologies (Grand Island, NY). Hema 3 Stat Pack used for Diff-Quik staining and IL-1β ELISA kit were purchased from ThermoFisher Scientific (Waltham, MA). IRDye 800CW- and IRDye 680RD-conjugated species-specific secondary antibodies were from LiCOR Biosciences (Lincoln, NE). Alexa Fluor 488- and 594-conjugated secondary antibodies for immunofluorescence microscopy were from Jackson ImmunoResearch Inc. (West Grove, PA). Caspase-1 inhibitor (Ac-YVAD-cmk) was purchased from Cayman Chemicals (Ann Arbor, MI). Fast Tissue/Tail PCR genotyping kit was purchased from EZ Bioresearch (St. Louis, MO). GoTaq Mastermix was purchased from Promega (Madison, WI).

Animals: All animal experiments were performed according to the protocols approved by the Institutional Animal Care and Use Committee of the Providence VA Medical Center for the humane care and use of laboratory animals and in compliance with local, state and federal regulations. The Providence VA Medical Center is an AAALAC international accredited organization. Male 8–10 week old C57BL/6 mice were purchased from Charles River Laboratories (Wilmington, MA). For genetically modified mice, both males and females were used. All mice were housed at the animal facility in the Providence VA Medical Center in standard conditions (12h/12 h light/dark cycle, 68–72 °F and a humidity of 30–70%) in ventilated racks fitted with automatic watering systems and fed with standard chow *ad libitum*.

IL-1β floxed mice (C57BL/6 background) and global IL-1β knockout mice (C57BL/6 background) were generated by Brown University Transgenic Core. Myeloid-specific Cre (LysM-Cre) mice (B6.129P2-Lyz2tm1(cre)Ifo/J) were purchased from the Jackson Laboratory (Bar Harbor, ME). Myeloid-specific IL-1β knockout mice (LysM-IL-1β^fl/fl) were generated by breeding IL-1β floxed mice with LysM-Cre mice. Genotyping was performed by PCR using primer pair (5' GTG GTC CTT GCA TGA AAC G 3'; 5' GTA TGG GAA GCC ATT GAG AGC 3'), which were made by Integrated DNA Technologies (Coralville, IA).

Cigarette smoke exposure of mice: As we previously published [22–24], mice were exposed to room air (RA) or cigarette smoke (CS) for either 6 h or 2 weeks for 6 h per day with cycles of 2 days on and 1 day off using a TE-10B rodent whole-body smoke exposure system (Teague Enterprises, Woodland, CA) and 3R4F reference cigarettes (University of Kentucky, Tobacco Research Institute, Lexington, KY). Each cigarette was puffed for 2 s, once every minute for a total of 8 puffs, at a flow rate of 1.05 l/min, to provide a standard puff of 35 cm³. The smoke machine was designed to produce and collect a mixture of side-stream (89%) and main-stream (11%) smoke. Three cigarettes were lit at a time, which produce and deliver an average of 150 mg/m³ of total suspended particles with approximately 20% F_{IO2} and 150 ppm of carbon monoxide into exposure chambers.

Instillation of P. aeruginosa: Mice were anesthetized with 3% isoflurane and given 50 μl of the laboratory strain of *P. aeruginosa* (PA103) by intratracheal instillation (non-surgical oro-tracheal). PA103 was a gift from Dr. Troy Stevens (University of South Alabama, Mobile, AL) and maintained according to previously described protocols [28]. Briefly, PA103 was grown on solid Lysogeny Broth (LB) agar plate for 16 h and then several colonies were resuspended in sterile saline. The concentrations of PA103 suspensions were determined by optical density (OD) at a wavelength of 600 nm using spectrophotometer (BioRad, Hercules, CA). The amounts of bacteria administered were based on the concentration of PA103 in suspension, aiming for 1×10^5 colony forming units (CFU). Quantitation of bacteria that mice received in each experiment was determined by standard plate counting of CFU grown on LB agar plates after serial dilutions and are presented in each figure legend. Control mice were administered an equal volume (50 μl) of sterile saline. After an 18-hour-7 day incubation period, lungs and BAL fluid were harvested for assessment of lung injury.

Changes in mouse body weight: Mouse body weights were recorded daily and change in body weight is presented as % of initial weight.

Lung Wet/Dry weight ratio: As we previously described [23], mice were euthanized with 120 mg/kg of pentobarbital and lungs were immediately harvested and weighed (wet weight). The lungs were dried for 72 h at 80 °C and the dried lungs were weighed. The wet/dry weight ratios were calculated.

Assessment of BAL protein, leukocytes, and bacterial load: Mice were anesthetized with a cocktail of 75 mg/kg of ketamine and 5 mg/kg of xylazine through intraperitoneal injection. A small incision was made in the trachea and a cannula attached to a 1 ml syringe containing sterile saline was inserted and secured. The lungs were then gently lavaged once with 600 μl of saline. Immediately after lavage, freshly collected BAL fluid was serially diluted and plated on LB agar plates. After overnight incubation, bacterial load in BAL was calculated by counting colony forming units (CFU) per ml of BAL fluid. Total white cells within

BAL fluid were counted using an automatic cell counter (a Bio-Rad TC20 Automated Cell Counter, Bio-Rad, Hercules, CA) gated within 8–20 μm. To determine BAL protein levels and numbers of individual types of white cells in BAL, BAL cells were separated from BAL fluid by centrifugation at 750g for 5min. BAL protein (the total protein content in the supernatant) was measured by DC protein assay. The cell pellets were resuspended in Red Blood Cell (RBC) Lysis Buffer (Roche, Basel, CH) to remove RBC and then centrifuged using a Cytospin. The cytospun cells were then stained by the Diff-Quik method to determine the percentages of macrophages, neutrophils, and lymphocytes in the BAL leukocyte population. The number of individual leukocytes in the BAL was calculated by determining the percentage of each cell type out of the total number of cells on the slide and multiplying this by the BAL total cell count.

Lung tissue fixation and freezing for cryosection: Lung tissues were fixed by inflating with melted 1% low melting agarose in 10% formalin at 25-cm water pressure for 5 min and then submerged in 10% formalin solution for an additional 2 h. The tissue was placed in 30% sucrose which was changed daily until the tissue sank to the bottom of the container. A plastic tray containing 2-methylbutane was placed in an ice bucket containing a few inches of liquid nitrogen. The tray was allowed to cool for several minutes and remained in the ice bucket submerged in the liquid nitrogen during the entire freezing protocol. In a labeled cryomold, OCT was added to just cover the bottom before placing the sample on top. Then, any remaining exposed tissue was covered with OCT. The cryomold was allowed to solidify in the tray with 2-methylbutane while avoiding letting it flow into the mold. The mold was stored in an airtight container at −80 °C until use.

Immunofluorescence microscopy: Lung tissues were fixed and frozen as described above. Immunofluorescence staining were performed on 5 μm frozen sections cut with a cryomicrotome (Leica CM1850, Leica Microsystems, Germany), mounted on SuperFrost Plus slides (Fisher Scientific, Pittsburgh, PA). Frozen tissue sections (5 μm) or cytospun dried slides were immunostained with single or co-stained with primary antibodies directly against HMGB1 (1:200), CD68 (1:100), p62 (1:100), NLRP3 (1:100) for 1 h. Slides were then incubated with Alexa 488 nm (green) or Alexa 594 nm (red) conjugated secondary antibodies (Molecular Probes, Eugene, OR) for 1 h. Sections were counterstained with DAPI/anti-fade mounting medium (Vector Laboratories). Images were captured with a Nikon microscope at 40X and 100X magnification.

Histology and Immunocytochemistry: Lungs were fixed by inflating with 10% formalin at 25-cm water pressure for 2 min, then submerged in 10% formalin solution for overnight, and then embedded with paraffin for sectioning. Sagittal sections (5 μm) were used for hematoxylin and eosin (H&E) staining and immunohistochemistry. Immunohistochemistry assessments for HMGB1, NLRP3 and p62 were performed after deparaffinization and rehydration in an ethanol series. The slides were blocked with 10% goat serum for 60 min, and then incubated with the primary antibodies for 60 min at room temperature. The sections were then incubated with secondary antibody (Vector labs) for 30 min at room temperature and developed with ImmPACT Vector Red (Vector Laboratories, SK-5105). All sections were counterstained with hematoxylin for nuclear, dehydrated in a sequence of graded alcohol/water mixtures and xylenes, and then covered with a cover slip. Images were acquired at 40X magnification with a Aperio Scanscope CS2 whole slide image system (Leica Biosystems, Nussloch, Germany). Ten areas representing upper, middle, and lower regions of each lung were analyzed using ImageScope software.

Electron Transmission Microscopy: Lung tissue was fixed in 2.5% glutaraldehyde overnight and then processed for electron microscopy. Images were acquired by the Philips 410 transmission electron microscope (Ledue Bioimaging facility, Brown University) and analyzed with AMT's imaging software.

Assessment of chemokines and cytokines: Lung tissue and cell-free BAL fluid were collected, snap-frozen in liquid nitrogen, and stored at −80 °C until use. Lung tissue was homogenized using the Sonics Vibra Cell VCX 130 (Newtown, CT). Equal amounts of proteins from lung homogenates or equal volume of BAL fluid were used for determination of levels of keratinocyte chemoattractant (KC), macrophage inflammatory protein-2 (MIP2), tumor necrosis factor (TNF)-α, interleukin (IL)-6, IL-1β, and IL10 by enzyme-linked immunosorbent assay (ELISA) kits per manufacturer recommendations. The levels of chemokines and cytokines in BAL fluid and lung tissue were expressed as pg/ml (BAL) and pg/mg protein (lung tissue), respectively.

Assessment of HMGB1 in BAL fluid: Equal volume (~400 μl) of cell free BAL fluid was concentrated using Amicon Ultra-0.5 mL Centrifugal Filters (10K device, Millipore Sigma) and then diluted in RIPA buffer. Laemmli buffer was then added to the concentrated sample and it was subjected to gel electrophoresis and immunoblot analysis.

Gel electrophoresis and immunoblot analysis: Tissue homogenates were dissolved in Laemmli buffer and proteins were resolved using SDS-PAGE electrophoresis. Proteins were transferred to PVDF membrane (Millipore) and immunoblotted with primary antibodies of interest, and fluorophore (IRDye 800CW and IRDye 680RD)-conjugated species-specific secondary antibodies. The fluorescence signals were captured and quantified by the LiCOR Odyssey® Imaging Systems.

Data analysis: The number of mice used in each experiment are indicated in figure legends. Data are presented as mean ± standard deviation (SD). The difference between two means was assessed using Student's T test. The differences among three or more means were assessed using two-way ANOVA multiple comparisons and Tukey's multiple comparisons test or Fisher's least significant difference post-hoc test using GraphPad Prism 8. For survival studies, Log-rank (Mantel-Cox) test was used for determining difference between groups. Differences among means are considered statistically significant when p < 0.05.

3. Results

3.1. CS pre-exposure exacerbated P. aeruginosa-induced acute lung injury

To characterize the effects of CS on ALI in mice infected by *P. aeruginosa*, we exposed mice to CS for 2 weeks, followed by infection with *P. aeruginosa* (strain: PA103, here after referred as PA) for 18 h before assessment of ALI. As expected, mice infected with PA for 18 h had a significant loss in body weight (Fig. 1a), increase in BAL protein content (Fig. 1b) and inflammatory cell infiltration (Fig. 1c–d). CS exposure for 2 weeks caused a significant reduction in mouse body weight (Suppl. Fig 1a), without significant effects in BAL protein content (Fig. 1b) or lung inflammatory cell infiltration (Fig. 1c–d). Interestingly, pre-exposure to CS for 2 weeks significantly exacerbated PA-triggered increase in BAL protein content (Fig. 1b) and lung inflammatory cell infiltration (Fig. 1c–d). To further characterize the effects of CS pre-exposure on PA-induced lung inflammation, we assessed levels of lung inflammatory cells and cytokines/chemokines. As expected, mice infected with PA for 18 h had a significant increase in BAL total leukocytes (Fig. 1e). The most abundant leukocytes increased were predominantly neutrophils (Fig. 1e). PA infection alone for 18 h had negligible effects on the number of BAL macrophages (Fig. 1e), but increased lung chemokines (KC and MIP2) and cytokines (TNF-α and IL-6) (Suppl. Fig. 1b, c, d, e). CS exposure for 2 weeks had no effect on the total number of BAL leukocytes, neutrophils or macrophages (Fig. 1e) or levels of lung chemokines/cytokines (Suppl. Fig. 1b, c, d, e). Though CS pre-exposure for 2 weeks did not have a statistically significant effect on PA-induced increase in BAL total cells or neutrophils (Fig. 1e), it exacerbated PA-triggered expression of lung chemokines/cytokines (Suppl. Fig. 1b, c, d, e).

Similar results were seen in mice acutely pre-exposed to CS for 6 h followed by PA infection. Specifically, mice exposed to CS for 6 h had a decrease in body weight (Suppl. Fig. 2a) without changes in lung wet/dry weight ratio (Suppl. Fig. 2b) or BAL protein content (Suppl. Fig. 2c).
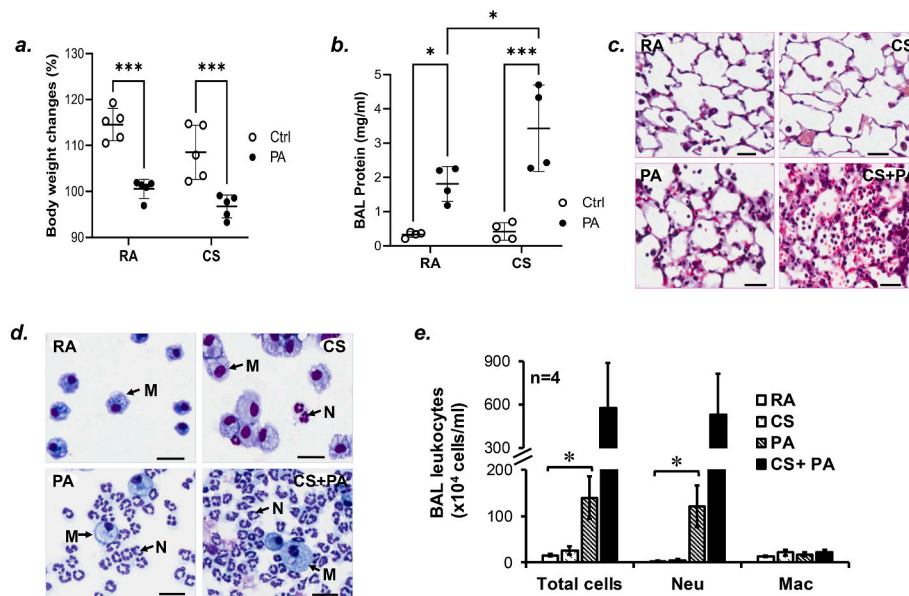
Fig. 1. Effects of two weeks of cigarette smoke pre-exposure on *P. aeruginosa*-induced acute lung injury. C57BL/6 adult male mice were exposed to room air (RA) or cigarette smoke (CS) for 2 weeks. One hour after the last CS exposure, mice were given 1.0×10^5 colony forming units (CFU) (determined based on the optical density of bacterial suspension) of *P. aeruginosa* (strain: PA103, referred as PA) in 50 μl saline or control (Ctrl, an equal volume of saline) by intratracheal instillation. The actual alive bacteria mice received were 1.8×10^5 CFU. 18 h after PA administration, changes in mouse body weight, as compared to that at the time immediately before entering the smoking study, were analyzed (a). Bronchoalveolar lavage (BAL) fluid was collected for assessment of BAL total protein levels by DC protein assay (b). Lung inflammatory cell infiltration was evaluated by lung histology with H & E staining (c). The total numbers of leukocytes in BAL fluid were assessed by an automatic cell counter. Individual leukocytes in BAL fluid were assessed by Diff Quik staining of the BAL cytospun slides (d). The numbers of individua leukocytes in BAL fluid were calculated based on the total numbers of BAL leukocytes and individual cell percentages (e). Panels c–d are representative images from at least 4 mice per group of each experiment. The scale bars = 30 μm. The arrows point to macrophages (Mac, M) or neutrophils (Neu, N). Data are presented as mean ± SD. Two-way ANOVA and Tukey's multiple comparison test was used to determine differences among means. *p < 0.05; ***p < 0.001.

However, pre-exposure to CS for 6 h exacerbated PA-induced increase in lung wet/dry weight ratio (Suppl. Fig. 2b) and BAL protein content (Suppl. Fig. 2c). Mice exposed to CS alone for 6 h slightly increased the numbers of BAL macrophages, with no effect on BAL neutrophils (Suppl. Fig. 2d) or chemokines/cytokines (Suppl. Fig. 2e–f). Though CS exposure for 6 h did not have a significant effect on PA-induced increase in BAL total cells or neutrophils (Suppl. Fig. 2d), it decreased the number of BAL macrophages upon presence of PA (Suppl. Fig. 2d) and exacerbated PA-induced production of TNF-α, IL-6 and IL-1β (Suppl. Fig. 2e–f). These results indicate that short term exposure to CS increases vulnerability to a secondary bacterial infection, resulting in increased lung injury.

High mobility group box 1 (HMGB1) is an evolutionarily conserved transcription factor and a prototypic alarmin mediating systemic inflammation [29]. Elevated HMGB1 can distinguish patients with ARDS from those without ARDS [30] and is independently associated with increased mortality in ARDS patients [31]. We found that neither CS exposure for 2 weeks nor PA infection alone had any significant effect on HMGB1 expression in either lungs (Suppl. Fig. 3a) or BAL macrophages (Suppl. Fig. 3b). However, CS/PA double-hit significantly enhanced the levels of HMGB1 in lungs (Suppl. Fig. 3a) and BAL macrophages (Suppl. Fig. 3b). *P. aeruginosa* has been shown to cause HMGB1 release in macrophages [32]. Consistently, we found that HMGB1 levels in BAL fluid of CS/PA-challenged mice were also significantly increased (Suppl. Fig. 3c–d). These results indicate that CS/PA double hit promotes HMGB1 expression in alveolar macrophages and extracellular release. These results also suggest that CS pre-exposure promotes PA-induced lung and systemic inflammation.

3.2. CS pre-exposure dampened lung bacterial clearance

CS has been shown to delay bacterial clearance in mice [33] and humans [34]. In this study, we also found that CS pre-exposure for either 6 h or 2 weeks significantly elevated bacterial load in BAL fluid (Fig. 2a). No bacteria was detectable in blood in any experimental groups (data not shown), indicating that there was no systemic dissemination of bacteria.

Sustained presence of bacteria in the lungs may cause lung cell death.

We found that PA infection increased caspase-3 cleavage, an effect that was not significantly altered by CS pre-exposure (Suppl. Fig. 4a, c). None of the exposures (CS, PA, or CS/PA) altered the levels of phosphorylation of mixed-lineage kinase domain-like protein (MLKL) at Thr357/Ser358, a marker of necroptosis (Suppl. Fig. 4b and c). These results suggest that conventional lung cell death is not a major contributor to CS exacerbation of PA-induced acute lung injury.

3.3. CS exacerbated PA-induced NLRP3 inflammasome activation in alveolar macrophages

NLRP3 inflammasome activation has been implicated in increased mortality in sepsis [35] and pneumonia [36]. To investigate if NLRP3 inflammasome is involved in CS primed PA-triggered ALI, we examined expression of NLRP3 inflammasome platform proteins (NLRP3, ASC, pro-caspase-1 and pro-IL-1β) and inflammasome activation (cleaved caspase-1 and mature IL-1β). We found that exposure to CS alone for 2 weeks had no effect on either NLRP3 inflammasome platform proteins or activation (Fig. 2b–d). PA infection for 18 h caused a robust increase in NLRP3 inflammasome platform proteins, including NLRP3, ASC, pro-caspase-1, and pro-IL-1β, and mature (cleaved) form of IL-1β (Fig. 2b–d). Though CS pre-exposure for 2 weeks did not affect PA-induced elevation of NLRP3, ASC, or pro-caspase-1 (Fig. 2b–c), it dramatically exacerbated PA-triggered increase in active caspase-1 (p20), pro-IL-1β, and mature IL-1β (Fig. 2b–d). Similar results regarding NLRP3 inflammasome platform protein expression were also seen in mice acutely pre-exposed to CS for 6 h followed by PA infection. Specifically, exposure to CS for 6 h had no effect on NLRP3 inflammasome platform proteins (NLRP3, ASC, pro-caspase-1) or activation (p20 caspase-1) (Suppl. Fig. 5a–b). As shown previously, PA infection for 18 h caused a robust increase in NLRP3 inflammasome platform proteins (NLRP3, ASC, pro-caspase-1) and p20 (active) caspase-1 (Suppl. Fig. 5a–b). Exposure to CS for 6 h had no effect on PA-induced expression of NLRP3, ASC, pro-caspase-1, or p20 caspase-1 (Suppl. Fig. 5a–b). These results suggest that duration of CS exposure may be important for robust NLRP3 inflammasome activation.

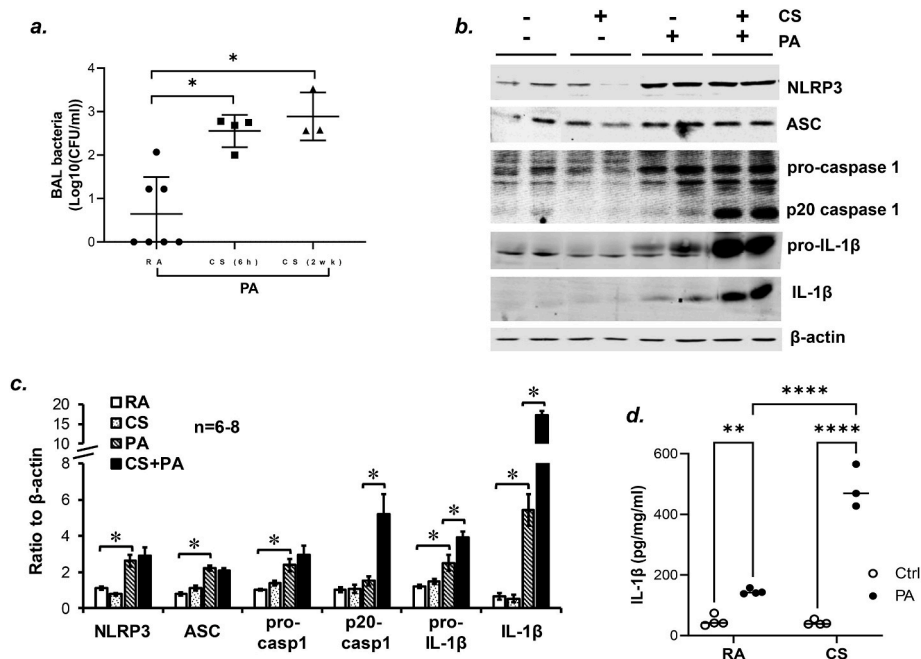To identify specific lung cells in which NLRP3 inflammasome was

Fig. 2. Effects of cigarette smoke on *P. aeruginosa*-triggered NLRP3 inflammasome activation. C57BL/6 adult male mice were exposed to RA, CS for 6 h or 2 weeks (a), or CS for 2 weeks (b–h). One hour after the last CS exposure, mice were given 1.0×10^5 CFU (determined based on the optical density of bacterial suspension) of PA103 (PA) in 50 μl saline or Ctrl (an equal volume of saline) by intratracheal instillation. The actual alive bacteria mice received were 1.8×10^5 CFU. 18 h after administration of PA, BAL fluid was collected for assessment of bacterial amount by counting colony forming units (CFU) (a). The data is presented as mean ± SD of Log10 (CFU/ml). 3–7 mice per experimental group were used. Lung homogenates from the experiment was prepared for assessment of NLRP3 inflammasome platform proteins (NLRP3, ASC, pro-caspase-1, and pro-IL-1β) and inflammasome activation (p20 caspase-1 and mature (cleaved) IL-1β) by immunoblot, using β-actin as a protein loading control (b). The relative levels of each protein of interest in each sample were determined by densitometry of their immunoblots normalized by immunoblots of respective protein loading controls. The densitometry values are presented as mean ± SD (c). 6–8 mice per experimental group were used. Two-way ANOVA and Tukey's multiple comparison test was used to determine differences among means. *p < 0.05. IL-1β levels in lung homogenates from this experiment were also assessed by ELISA (d). Data are presented as mean ± SD. Two-way ANOVA and Tukey's multiple comparison test was used to determine differences among means. **p < 0.01; ****p < 0.0001. The cytospun slides of BAL leukocytes (e) and cryosections of lung tissue (f, h) from these experiments were prepared for immunofluorescence microscopy to examine NLRP3 expression/localization (green) in either AM (CD68+, red; e, f) or lung endothelial cells (von Willebrand factor (vWF+), red; h). DAPI was used to stain nuclei (blue). Panels e, f, h are representative images for each experimental group. Scale bar = 15 μm. The arrows in panels e–f indicate alveolar macrophages (M) and the arrows in panel h indicate lung endothelial cells (EC). The percentage of AM expressing NLRP3 over the total AM counted are presented as mean ± SD (g). Five slides at 40X and five slides at 100X per mouse lung tissue or BAL cytospun slides were used to count AM. Two-way ANOVA and Tukey's multiple comparison test was used to determine differences among means. ****p < 0.0001. (For interpretation of the references to colour in this figure legend, the reader is referred to the Web version of this article.)

activated, we assessed NLRP3 expression in lung sections and BAL cytospin slides by immunofluorescence microscopy, using cluster of differentiation 68 (CD68) and von Willebrand factor (vWF) to label lung macrophages and endothelial cells, respectively. We found that NLRP3 expression was undetectable in any lung cells of mice exposed to RA or CS alone for 2 weeks (Fig. 2e, f, h). PA infection for 18 h significantly increased NLRP3 expression predominantly in alveolar macrophages (AM) (Fig. 2e, f, g). Pre-exposure to CS for 2 weeks did not have any significant effect on PA-induced NLRP3 expression in AM (Fig. 2e, f, g). NLRP3 was not expressed in lung endothelial cells (Fig. 2h) or BAL neutrophils (Fig. 2f) in mice challenged by PA alone. However, CS/PA double-hit seems to slightly increase NLRP3 expression in endothelial cells (Fig. 2h). Our results suggest that CS/PA activates NLRP3 inflammasome predominantly in AM and possible lung endothelial cells.

3.4. Inhibition of caspase-1 attenuated CS/PA double-hit-induced ALI and improved bacterial clearance and animal survival

To address the role of NLRP3 inflammasome activation in CS/PA double-hit-induced ALI, we first tested the effect of inhibition of inflammasome by a pharmacological inhibitor of caspase-1, N-Ac-Tyr-Val-Ala-Asp-chloromethyl ketone (Ac-YVAD). Since NLRP3 inflammasomes were not activated during CS exposure, Ac-YVAD was given to

mice after 2 weeks of CS exposure and 1 h before administration of PA. We found that 10 mg/kg of Ac-YVAD attenuated CS/PA-induced inflammasome activation, as indicated by attenuated release of mature IL-1β into BAL fluid (Fig. 3a). Ac-YVAD caused a mild but insignificant attenuation of PA-induced IL-1β release (Fig. 3a). Importantly, Ac-YVAD significantly attenuated CS/PA-, but not PA-, induced increase in BAL protein content (Fig. 3b), and rescued CS/PA-, but not PA-, induced reduction of AM (Fig. 3c). Though Ac-YVAD had no effects on PA- or CS/PA-induced increases in BAL total cells, neutrophils or lymphocytes (Fig. 3d–f), it significantly blunted CS/PA-, but not PA-, induced increases in KC, TNF-α, and IL-6 (Fig. 3g–i). Ac-YVAD did not change PA- or CS/PA-induced IL-10 expression (Fig. 3j). In addition, Ac-YVAD significantly improved lung bacterial clearance (Fig. 3k) and animal survival (Fig. 3i) from PA or CS/PA injury. These results indicate that NLRP3 inflammasome activation contributes to CS/PA-induced ALI and mortality.

3.5. Global and myeloid-specific IL-1β knockout attenuated CS/PA-induced ALI in female mice

IL-1β is activated by active caspase-1 upon inflammasome activation. To address the role of IL-1β in CS/PA-induced ALI, we used global IL-1β knockout mice and age-matched wild type littermates. Global knockout
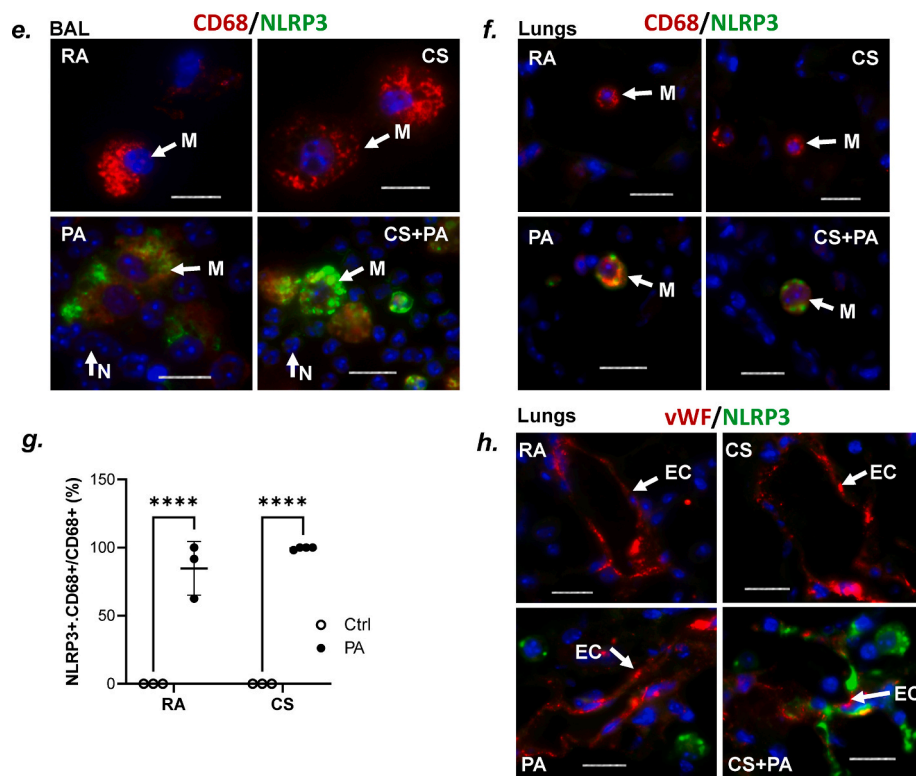
Fig. 2. (*continued*).

of IL-1β was confirmed by genotyping (Fig. 4a) and Western blot (Fig. 4b). Similar to the effect of caspase-1 inhibitor, global knockout of IL-1β in female mice challenged by CS/PA had a significant lower BAL protein content (Fig. 4c), less BAL inflammatory cells (Fig. 4d), and less lung bacterial burden (Fig. 4e), as compared to its wild type control female littermates. To our surprise, this protection was not observed in global IL-1β knockout male mice (Fig. 4c–e), suggesting a sex-differential effect of IL-1β in CS/PA-triggered acute lung injury.

Since NLRP3 is induced by PA or CS/PA predominantly in AM, we next addressed the effect of blocking NLRP3 inflammasome signaling by using myeloid-specific IL-1β knockout mice on PA- and CS/PA-induced lung injury. We generated myeloid-specific IL-1β knockout mice by mating LysM$^{Cre/Cre}$ mice with IL-1β$^{flox/flox}$ mice. LysM^{Cre}-IL-1β^{flox} was confirmed by genotyping (Fig. 5a). To confirm if IL-1β was knocked out in alveolar macrophages, we collected BAL cells from untreated LysM^{Cre}-IL-1β^{flox} mice and wild type control mice. The BAL cells were composed of 80.60 ± 2.45% of alveolar macrophages, 19.02 ± 2.46% neutrophils, and a tiny fraction of lymphocytes. By ELISA assay, we found that IL-1β was significantly reduced in BAL cells of LysM^{Cre}-IL-1β^{flox} mice (Fig. 5b). Since we did not observe any phenotypic difference between LysM$^{Cre/Cre}$-IL-1β and LysM$^{Cre/+-}$IL-1β mice, equal numbers of these mice were used. Similar to results observed in global IL-1β knockout female mice, myeloid-specific IL-1β knockout female mice were also protected from CS primed PA-triggered lung edema (Fig. 5c). Again, this protection was not observed in myeloid-specific IL-1β knockout male mice (Fig. 5c), suggesting a sex-differential effect of myeloid-specific IL-1β in CS/PA-triggered acute lung injury. We also assessed effects of myeloid-specific IL-1β knockout on PA- and CS/PA-induced long-term outcomes, which were evaluated by total protein content, bacterial burden and total inflammatory cells in BAL fluid 7 days after PA infection, as well as animal survival over 7 days. We found that BAL protein levels were significantly lower in myeloid-specific IL-1β knockout female mice, as compared to its wild type female controls, in either PA or CS/PA injury models (Fig. 5d). This protection was also not seen in myeloid-specific IL-1β knockout male mice (Fig. 5d). We found that myeloid-

specific IL-1β knockout completely cleared BAL bacteria 7 days post infection in either PA- or CS/PA injury models in both sex (Fig. 5e). We noted that the numbers of BAL inflammatory cells at 7 days post infection returned to normal levels in either wild type or myeloid-specific IL-1β knockout of either male or female in either PA or CS/PA injury models (Fig. 5f).

We next assessed animal survival from PA or CS/PA challenges and found that male mice had significantly higher mortality, as compared to female mice, after infection with PA (Fig. 5g). Myeloid-specific IL-1β knockout exacerbated PA-triggered mortality in both sexes (Fig. 5g). Myeloid-specific IL-1β knockout also increased mortality at 4–7 days post PA challenge following 2 weeks of CS exposure (Fig. 5h). These results suggest that other factors may contribute to increased mortality in myeloid-specific IL-1β knockout mice.

3.6. CS exacerbated PA-induced mitochondrial damage and impaired mitophagy flux in alveolar macrophages

Mitophagy has been shown to regulates NLRP3 inflammasome activation in macrophages [37,38]. To begin to understand mechanism underlying NLRP3 inflammasome activation, we first examined the effects of CS and PA on mitochondrial damage in AM by transmission electrical microscopy. We found that mitochondria of AM from control mice displayed typical mitochondrial morphology (smooth outer membrane and inner membrane folding into cristae) (Fig. 6a). Exposure to CS alone for 2 weeks did not change mitochondrial morphology of AM, whereas PA alone for 18 h reduced the length of cristae of mitochondria in AM (Fig. 6a). Mice exposed to CS for 2 weeks and then infected with PA for 18 h (CS/PA) displayed swollen, rounded, or fragmented mitochondria with loss of mitochondrial cristae, and accumulation of double-membraned large autophagosome-like structures in AM (Fig. 6a–b). CS/PA double hit also caused condensed abnormal lysosomes in AM (Fig. 6a).

Mitophagy serves to maintain mitochondria homeostasis by removing damaged or fragmented mitochondria [26,39]. To determine
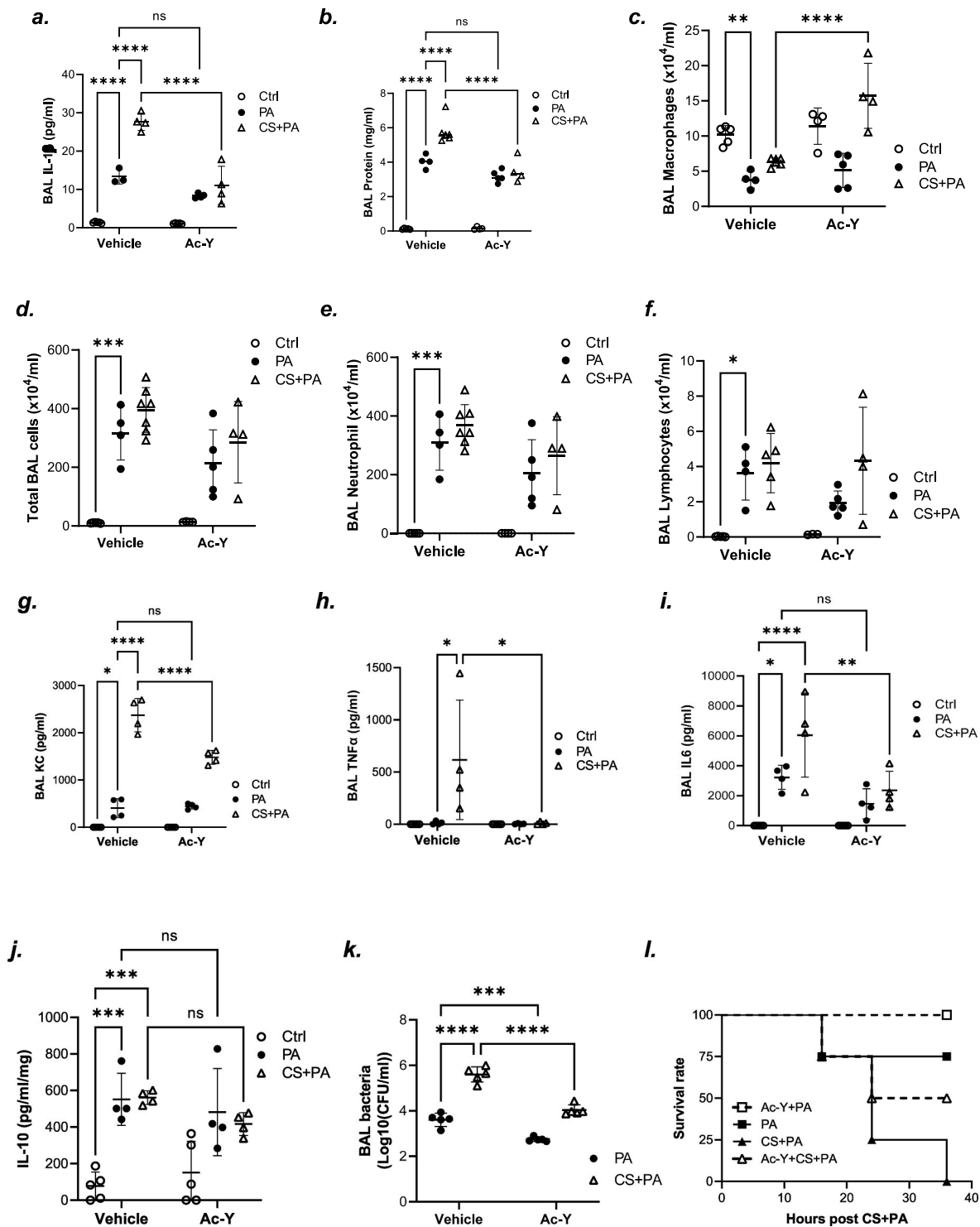
Fig. 3. Effects of pharmacological inhibition of caspase-1 on PA- and CS/PA-induced acute lung injury. C57BL/6 adult male mice were exposed to RA or CS for 2 weeks. One hour after the last CS exposure, mice were administered a caspase-1 inhibitor, Ac-YVAD-cmk (Ac–Y) at a dose of 10 mg/kg or vehicle intraperitoneally. One hour later, mice were given 1.0×10^5 CFU (determined based on the optical density of bacterial suspension) of PA103 (PA) in 50 μl saline or Ctrl (an equal volume of saline) by intratracheal instillation. The actual alive bacteria mice received were 3.5×10^5 CFU. 18 h after administration of PA, BAL fluid was collected for assessment of inflammasome activation by measuring mature IL-1β levels in cell-free BAL fluid by ELISA (a), BAL total protein levels (b), BAL inflammatory cells (c–f), BAL chemokine/cytokines (g–j), and BAL bacterial loads (k). Animal survival was recorded up to 36 h after administration of PA in a separate set of mice (l). 4–7 mice per experimental group were used. Data are presented as mean ± SD. Two-way ANOVA and Tukey's multiple comparison test was used to determine differences among means for studies other than survival study, in which Log-rank (Mantel-Cox) test was used for determining difference among groups. *p < 0.05; **p < 0.01; ***p < 0.001; ****p < 0.0001; NS: not significant.
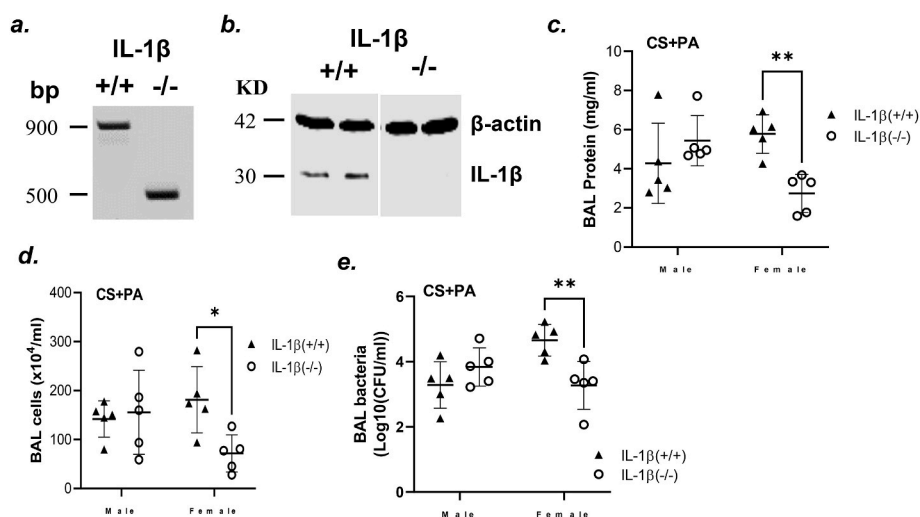
Fig. 4. Effects of global IL-1β knockout on CS/PA double-hit-induced acute lung injury. Adult male and female global IL-1β knockout (IL-1β−/−) and age-matched wild type littermates (IL-1β+/+) were used. Knockout of IL-1β was confirmed by both genotyping (a) and immunoblotting of lung homogenates (b). These mice were exposed to RA or CS for 6 h, followed by intratracheal instillation of 1×10^5 CFU of PA (determined based on optical density of bacterial suspension) in 50 μl saline or Ctrl (an equal volume of saline). The actual alive bacteria mice received as following: 0.98×10^5 CFU for male, 1.4×10^5 CFU for female. 18 h later, BAL fluid was collected for assessment of BAL total protein levels (c), BAL total inflammatory cells (d), and BAL bacterial loads (e). Data are presented as mean ± SD. Unpaired *t*-test was used to determine the difference between wild type and IL-1β knockout mice with the same challenge. *p < 0.05; **p < 0.01.
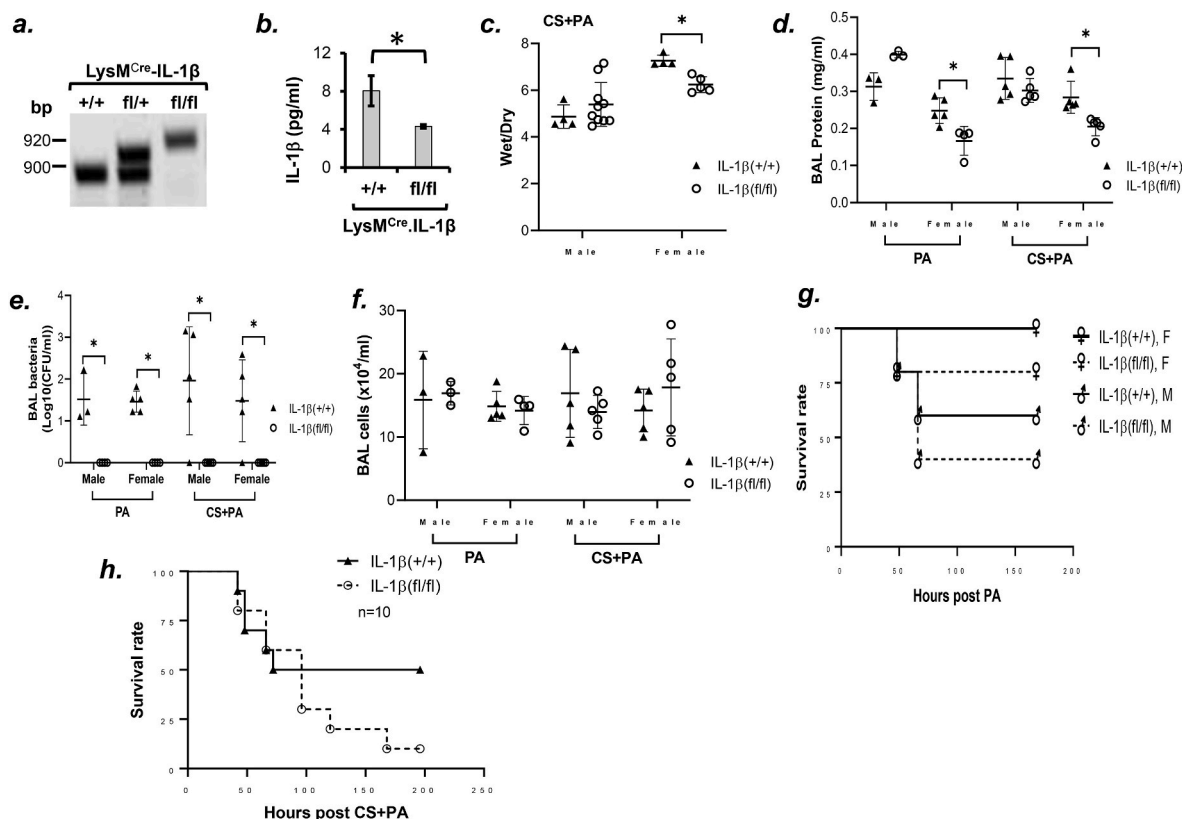

Fig. 5. Effects of myeloid-specific IL-1β knockout on CS/PA double-hits-induced acute lung injury and animal survival. Myeloid-specific IL-1β knockout (LysM^Cre-IL-1β^fl/fl) and wild type littermate (LysM^Cre-IL-1β^+/+) mice were generated using LysM^Cre/Cre mice mated with IL-1β^fl/fl mice. Myeloid-specific knockout of IL-1β was confirmed by genotyping (a) and ELISA analysis of BAL inflammatory cells of these mice (b). Adult male and female myeloid-specific IL-1β knockout (LysM^Cre-IL-1β^fl/fl) and age-matched wild type littermates (LysM^Cre-IL-1β^+/+) were exposed to RA or CS for 6 h, followed by intratracheal instillation of 1×10^5 CFU of PA (determined based on optical density of bacterial suspension) in 50 μl saline or Ctrl (an equal volume of saline). The actual alive bacteria mice received were 4.5×10^5 CFU for male and 3.5×10^5 CFU for female. 18 h later, lung tissue was collected for assessment of lung wet/dry weight ratio (c). 7 days after PA administration, BAL fluid was collected for assessment of BAL total protein levels (d), BAL total inflammatory cells (e), and BAL bacterial loads (f). Animal survival within 7 days post infection was recorded and analyzed (g). 3–10 mice per experimental group were used. Data are presented as mean ± SD. Unpaired *t*-test was used to determine the difference between wild type and IL-1β knockout mice with the same challenge. For survival studies, Log-rank (Mantel-Cox) test was used for determining difference between groups. *p < 0.05.

if mitophagy is activated or impaired in response to mitochondrial damage, we examined the effects of CS and PA on mitophagy in lungs and AM. We found that exposure of mice to CS alone for 2 weeks did not have any significant effects on mitophagy, as assessed by its markers, including parkin, PINK1, LC3B-II, Beclin, and p62 (Fig. 6c–f). Infection of mice with PA alone for 18 h significantly enhanced protein levels of Parkin in lung homogenates, with no effect on PINK1, conversion of LC3B–I to LC3B-II, and Beclin1; effects that were not altered by CS
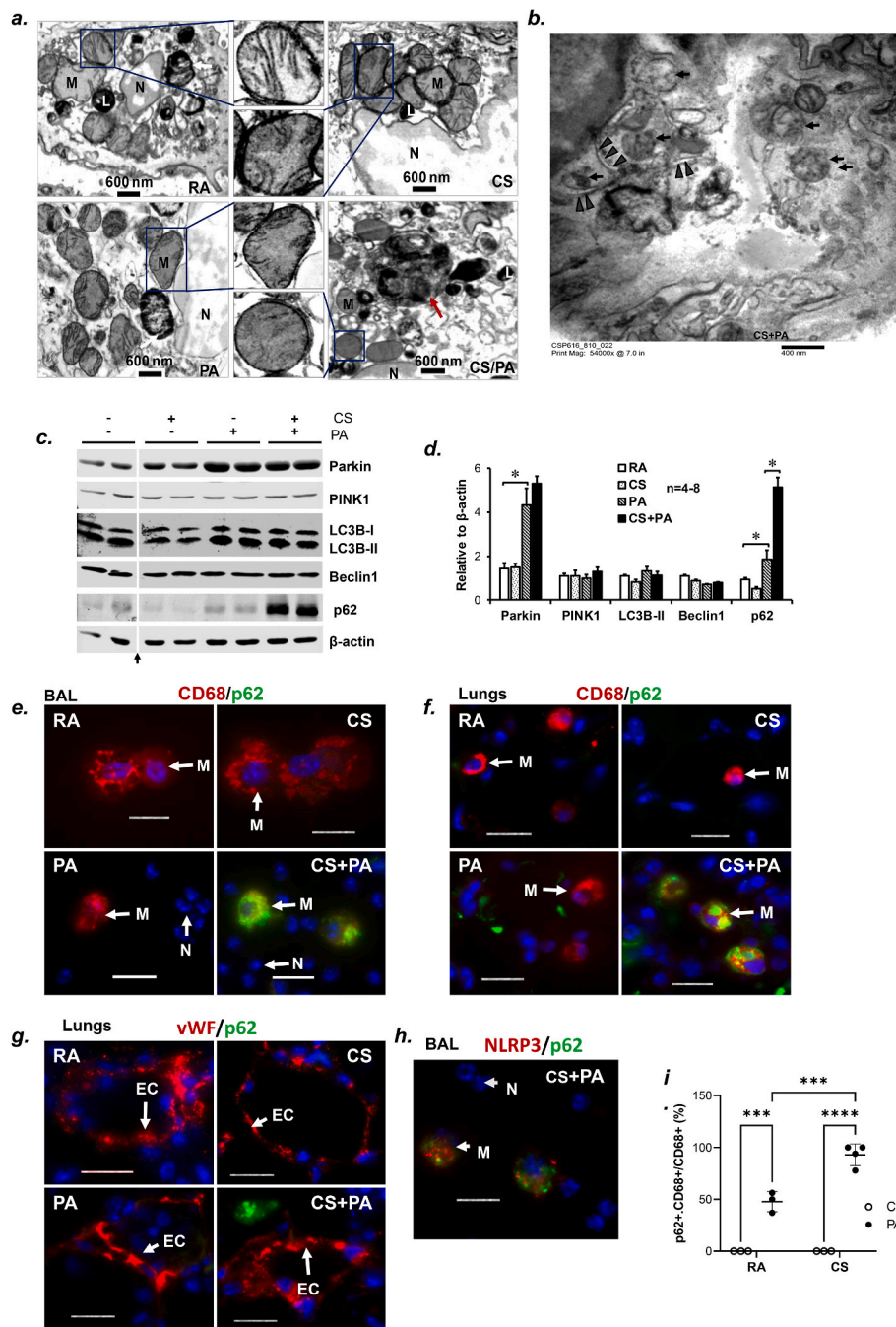
Fig. 6. Effects of CS/PA double-hit on mitochondrial injury and mitophagy. C57BL/6 adult male mice were exposed to RA or CS for 2 weeks. One hour after the last CS exposure, mice were given 1.0×10^5 CFU (determined based on the optical density of bacterial suspension) of PA103 (PA) in 50 µl saline or Ctrl (an equal volume of saline) by intratracheal instillation. The actual alive bacteria mice received were 1.8×10^5 CFU. 18 h after administration of PA, lung tissue was collected and fixed for assessment of mitochondrial morphology of alveolar macrophages by TEM (a–b). Arrows and triangles in panel b point to injured mitochondria and double-membraned autophagosomes, respectively. Panels a–b represent images from 3 mice per group. Mitophagy was assessed by levels of Parkin, PINK1, LC3B, Beclin1, and p62 in lung homogenates by immunoblot, using β-actin as a protein loading control (c). The relative levels of each sample for each protein of interest were determined by densitometry of their immunoblots normalized by immunoblots of respective protein loading controls. The densitometry values are presented as mean ± SD (d). 4–8 mice per experimental group were used in panels c–d. Two-way ANOVA and Tukey's multiple comparison test was used to determine differences among means. *p < 0.05. The cytospun slides of BAL leukocytes (e, h) and cryosections of lung tissue (f–g) from these experiments were prepared for immuno-fluorescence microscopy to examine p62 expression/localization (green) in lung CD68$^+$ macrophages (red; panels e–f) and in lung endothelial cells (vWF+) (red; panel g), as well as co-expression of p62 (green) and NLRP3 (red). Panels e–h are representative images. Scale bar = 15 µm. The arrow in panel b indicates removal of 2 irrelevant samples from the original gels. The arrows in panels e–h indicate alveolar macrophages (M), neutrophils (N) or endothelial cells (EC). The percentage of AM expressing p62 over the total AM counted are presented as mean ± SD (i). Five slides at 40X and five slides at 100X per mouse lung tissue or BAL cytospun slides were used to count AM. Two-way ANOVA and Tukey's multiple comparison test was used to determine differences among means. ***p < 0.001; ****p < 0.0001. (For interpretation of the references to colour in this figure legend, the reader is referred to the Web version of this article.)

pre-exposure (Fig. 6c–d). These results suggest that CS does not alter PA-induced steady-state mitophagy.

p62 has been recognized as a marker for impaired mitophagy flux [27]. Accumulation of autophagosomes in AM (Fig. 6a–b) suggests possible impairment of mitophagy flux. Thus we assessed p62 levels in lungs and AM. We found that CS exposure alone slightly decreased p62 protein levels in lungs (Fig. 6c–d). PA elevated p62; an effect that was dramatically exacerbated by CS pre-exposure (Fig. 6c–d). To identify specific lung cells in which p62 accumulated, we assessed p62 localization in lung sections and BAL cytospin slides by immunofluorescence microscopy, using CD68 and vWF to label AM and lung endothelial cells, respectively. We found that p62 was not detectable in any lung cells of mice exposed to RA or CS alone (Fig. 6e–g). CS dramatically exacerbated PA-induced p62 accumulation in AM (Fig. 6e–h, i), but not in lung endothelial cells (Fig. 6g) or neutrophils (Fig. 6e–f, h). It appears that CS/PA double hit caused co-expression of p62 with NLRP3 in AM, but not in neutrophils (Fig. 6h). These results suggest that CS/PA causes impairment of mitophagy flux in AM.

4. Discussion

In this study, we characterized the exacerbating effects of both a brief and prolonged pre-exposure to CS in *P. aeruginosa*-triggered ALI in a preclinical animal model. We also show that CS impaired *P. aeruginosa*-induced mitophagy flux, promoted p62 accumulation, and exacerbated *P. aeruginosa*-triggered mitochondrial damage and NLRP3 inflammasome activation in alveolar macrophages; an effect associated with increased acute lung injury and mortality. Pharmacological inhibition of caspase-1, a component of inflammasome, attenuated CS primed *P. aeruginosa*-triggered acute lung injury and improved animal survival. We also noted sex-differential effect of IL-1β in CS primed *P. aeruginosa*-triggered acute lung injury.

Cigarette smoking is a risk factor for pneumonia [5,6] and ARDS in patients with trauma [8], sepsis [9], surgery [10,11], blood transfusions [12], and lung transplantation [13]. Pneumonia is also a risk factor for ARDS [19]. However, there is no concrete epidemiologic evidence demonstrating whether cigarette smoking increases the risk for ARDS in patients with pneumonia. Using an animal model of pneumonia caused by *P. aeruginosa*, we found that both a brief (6 h) and prolonged (2 week) CS pre-exposure exacerbated *P. aeruginosa*-induced ALI. Our data suggest an important role of cigarette smoking in the etiology/pre-disposition to ARDS in subjects with pneumonia. Though both acute and prolonged CS exposure exacerbated PA-induced ALI, the duration of CS exposure influences the overall outcomes, with longer exposure having more severe effect on PA-induced ALI.

Why otherwise healthy smokers develop ARDS in response to infection or trauma is unknown. *P. aeruginosa* has multiple virulence factors and type 3 secretion systems (T3SS) which inject cytotoxins into the cytoplasm of host cells, thus causing tissue injury. CS has been shown to delay bacterial clearance in mice [33] and enhance bacterial biofilm formation in humans [34]. Other studies, however, showed that CS exposure transiently enhances lung bacterial clearance [40]. In this study, we found that CS pre-exposure increased lung bacterial burden, indicating defective bacterial clearance, which may contribute to or prolong *P. aeruginosa*-induced ALI. AM are the first line of defense by phagocytosis of external pathogens and apoptotic neutrophils [41] and secretion of M2 anti-inflammatory cytokines. CS has been shown to delay AM phagocytosis of pathogens [33,42]. In this study, we found that CS exacerbated *P. aeruginosa*-induced lung edema, cytokine storm, as indicated by dramatic elevation of TNF-α, IL6, IL-1β, and HMGB1 in BAL fluid; events that were significantly attenuated by caspase-1 inhibitor. Inhibition of caspase-1 also rescued diminishment of AM caused by CS/PA. Thus, it is possible that CS pre-exposure dampens lung bacterial clearance and causes cytokine storm by impairing AM function.

Neutrophils contribute to bacterial clearance, however, excessive neutrophil infiltration also causes bystander tissue injury. We found that

CS did not significantly increase *P. aeruginosa*-triggered lung neutrophil infiltration. Additionally, neither CS nor *P. aeruginosa* infection caused significant lung cell apoptosis or necroptosis. Our data suggest that neutrophil infiltration and lung cell apoptosis or necroptosis may not be important contributors to CS primed *P. aeruginosa*-triggered ALI. *P. aeruginosa* has recently been shown to induce lipid peroxidation, leading to ferroptotic cell death in human airway epithelial cells [43–45]. Future studies are needed to address if lipid peroxidation and ferroptotic cell death contributes to CS priming PA-triggered ALI.

We have previously shown that *P. aeruginosa* activates NLRP3 inflammasome [46]. However, it is unknown if CS influences *P. aeruginosa*-induced NLRP3 inflammasome activation. In this study, we found that *P. aeruginosa* alone robustly increased expression of NLRP3 inflammasome platform proteins (NLRP3, ASC, pro-caspase-1); effects that were not altered by either acute or prolonged CS pre-exposure. *P. aeruginosa* alone only moderately activated inflammasome (p20 caspase-1 and IL-1β) in AM. However, prolonged, not acute, CS pre-exposure dramatically intensified *P. aeruginosa*-triggered inflammasome activation (p20 caspase-1 and IL-1β) in AM. Importantly, inhibition of caspase-1 significantly attenuated 2 weeks of CS exposure primed *P. aeruginosa*-triggered ALI and improved lung bacterial clearance and animal survival. Our results suggest that activation of caspase-1 due to NLRP3 inflammasome activation in AM mediates CS priming *P. aeruginosa*-triggered ALI, partially by dampening AM-dependent bacterial clearance and increasing cytokine storm, as depicted in Fig. 7.

Mice deficient in IL-1 receptor [47] or IL-18 [48] were protected from acute *P. aeruginosa* pneumonia. Similarly, we found that both global and myeloid-specific IL-1β knockout in female mice attenuated CS primed *P. aeruginosa*-triggered ALI and significantly enhanced lung bacterial clearance. However, this protection of IL-1β knockout against CS primed *P. aeruginosa*-induced acute lung injury was only observed in female mice, but not in male mice. The underlying mechanism of this sex-dependent differences remains unknown and should be addressed in future studies. Women have decreased hospitalization for pneumonia or Covid-19 likely due to estrogen [49]. Female mice have also been shown to have greater resistance to pneumococcal pneumonia with greater bacterial clearance, diminished lung inflammation, and better survival [50]. The underlying mechanism has been linked to estrogen-mediated activation of lung macrophage nitric oxide synthase-3 [50]. Consistently, in this study, we found that wild type female mice had significantly lower mortality, as compared to wild type male mice, after CS primed *P. aeruginosa* infection. There is a discrepancy between caspase-1 inhibitor and IL-1β knockout in protection against CS primed *P. aeruginosa*-induced acute lung injury in male mice. We do not understand this surprising but interesting observation. Caspase-1 can activate both IL-1β and IL-18. It may be possible that IL-18 will mediate caspase-1 signaling when IL-1β is knockout in male mice. In contrast, IL-18 may not compensate for IL-1β in female mice when it is knockout. If that is true, we would anticipate that inhibition of caspase-1 in either male or female would protect against CS priming *P. aeruginosa*-induced ALI, but inhibition of IL-1β would protect against CS priming *P. aeruginosa*-induced ALI in female only, not male. This hypothesis may be tested in future. IL-1β has been shown to play a central role in mediating sex-based differences in Kawasaki Disease [51]. Gender difference in IL-1 receptor antagonist (IL-1ra) gene polymorphism affects IL-1β and IL-1ra levels and this difference might be one of the causes for the sex differences in immune response observed in various conditions, such as autoimmune diseases [52]. Nonetheless, future studies is needed to address this issue.

Both global and myeloid-specific IL-1β knockout mice had enhanced lung bacterial clearance and attenuated acute lung injury and cytokine storm upon challenges by CS primed *P. aeruginosa* infection. However, to our surprise, myeloid-specific IL-1β knockout mice had increased mortality between 4 and 7 days post *P. aeruginosa* infection with or without 2 weeks of CS pre-exposure. Our observations are consistent with a
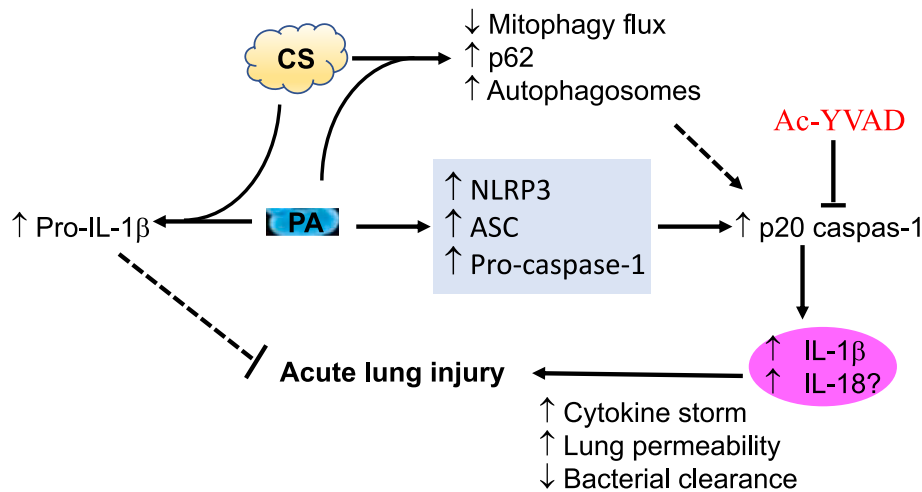
Fig. 7. The proposed mechanism underlying CS priming of PA-triggered acute lung injury. CS: cigarette smoke exposure; PA: *P. aeruginosa*. Solid lines define as demonstrated pathways and dotted lines defined as suggested pathways.

previous report that IL-1 receptor knockout mice were more susceptible to a chronic *Pseudomonas* pneumonia [53]. In addition, IL-1 receptor antagonist was ineffective or worsened lung injury in clinical trials [54, 55]. These findings suggest that some yet unidentified mechanism(s) caused increased long term mortality in IL-1β knockout mice. The discrepancy between acute protection verse adverse long term survival may attribute to multifunctionality of IL-1β. IL-1β knockout attenuated CS primed *P. aeruginosa*-triggered ALI likely by blocking NLRP3 inflammasome pathway, as depicted in Fig. 7. IL-1β increases lung alveolar-vascular permeability and promotes production of cytokine storm [56]. This may explain why knockout of IL-1β protects against lung edema. On the other hand, IL-1β can increase expression of inter-cellular adhesion molecule-1 (ICAM-1) and vascular cell adhesion molecule-1 (VCAM-1) in all organs, with strongest induction in the lungs [57]. IL-1β also promotes endothelial differentiation and angiogenesis in lung mesenchymal stem cells (MSC), suggesting a potential role of IL-1β in tissue repair [58]. In this study, we found that PA alone slightly increased pro-IL-1β expression; an effect dramatically exacerbated by two weeks of CS pre-exposure. It is possible that induction of pro-IL-1β by PA or CS/PA is a protective tissue repair mechanism to resolve lung injury, as depicted in Fig. 7. Therefore, it is possible that IL-1β knockout increased mortality due to inhibition of IL-1β-mediated tissue repair. We certainly can't rule out the possibility of compensatory mechanism due to constitutively IL-1β knockout.

Our data show that CS did not alter *P. aeruginosa*-induced steady-state mitophagy (Parkin and LC3II), but promoted *P. aeruginosa*-induced accumulation of p62 and autophagosomes in AM. These data suggest that CS impairs *P. aeruginosa*-induced mitophagy flux. p62 binds to damaged mitochondria and LC3, and is degraded in lysosomes as an outcome of functional mitophagy [59]. Impairment of mitophagy flux results in p62 accumulation, which increases nuclear factor (NF)-kB signaling to promote inflammation activation [60]. Cytoplasmic accumulation of p62 aggregates also directly activates NLRP3 inflammasome in human macrophages [61]. In this study, we showed that two weeks of CS exposure exacerbated *P. aeruginosa*-induced mitochondrial damage and p62 accumulation in alveolar macrophages; an effect associated with inflammasome activation (increased p20 caspase-1 and mature IL-1β). On the other hand, 6 h of CS pre-exposure did not exacerbate *P. aeruginosa*-induced inflammasome activation; an effect also associated with no exacerbation of p62 accumulation. Thus, these data revealed an association of mitochondrial damage and p62 accumulation with inflammasome activation in AM. Additionally, p62 levels were dramatically elevated in alveolar macrophages of human subjects died from stroke or trauma, which are risk factors for ARDS, as compared to

that of participants who died from other causes of brain death (unpublished data). Future studies are needed to address if impaired mitophagy flux, mitochondrial damage, and p62 accumulation in AM mediate CS/PA-induced NLRP3 inflammasome activation and ALI.

This study has some limitations. The short (6 h) and longer (2 weeks) durations of tobacco smoke exposure of mice were arbitrarily chosen and may not reflect changes in lungs of adult human smokers who are considered otherwise healthy. Because it is impossible to know CFU of bacteria before giving it to mice and because the optical density of *P. aeruginosa* is not well correlated with CFU, there is an unavoidable variability of *P. aeruginosa* among experiments though we aimed for 1×10^5 CFU of *P. aeruginosa* for all experiments. However, since each experiment has its own control group, we believe this variability should not impact overall conclusions. Another limitation is related to mechanism underlying sex-dependent effect of IL-1β knockout, which remains to be determined by future studies.

In summary, we demonstrate that CS exposure primes for *P. aeruginosa*-induced acute lung injury in mice. This priming appears to impair mitophagy flux, increase p62, and activate NLRP3 inflammasome in AM after *P. aeruginosa* infection. Pharmacological inhibition of caspase-1 attenuated CS/PA double hit-induced ALI and improved animal survival. We speculate that targeting selected components (e.g. caspase-1) of the inflammasome may be a better strategy to treat ARDS patients who have a history of smoking.

Author contributions

Conception and Design: QL; Data acquisition and analysis: AW, ZW, XW, MK, CG, QL, CM, EC; Data Interpretation: QL, SR; Drafting the manuscript: QL, AW; Revise the manuscript: QL, SR, LBW, AA, AM, GC, FS.

Declaration of competing interest

None.

Data availability

Data will be made available on request.

Acknowledgments

Appendix A. Supplementary data

Supplementary data to this article can be found online at https://doi.org/10.1016/j.redox.2022.102467.

References

[1] The Health Consequences of Smoking-50 Years of Progress: A Report of the Surgeon General, 2014. Atlanta (GA).

[2] K.J. Hoggatt, K. Lehavot, M. Krenek, C.A. Schweizer, T. Simpson, Prevalence of substance misuse among US veterans in the general population, Am. J. Addict. 26 (2017) 357–365.

[3] C. Feldman, R. Anderson, Cigarette smoking and mechanisms of susceptibility to infections of the respiratory tract and other organ systems, J. Infect. 67 (2013) 169–184.

[4] A.A. Lugade, P.N. Bogner, T.H. Thatcher, P.J. Sime, R.P. Phipps, Y. Thanavala, Cigarette smoke exposure exacerbates lung inflammation and compromises immunity to bacterial infection, J. Immunol. 192 (2014) 5226–5235.

[5] L. Arcavi, N.L. Benowitz, Cigarette smoking and infection, Arch. Intern. Med. 164 (2004) 2206–2216.

[6] L.E. Crotty Alexander, S. Shin, J.H. Hwang, Inflammatory diseases of the lung induced by conventional cigarette smoke: a review, Chest 148 (2015) 1307–1322.

[7] J. Almirall, J. Blanquer, S. Bello, Community-acquired pneumonia among smokers, Arch. Bronconeumol. 50 (2014) 250–254.

[8] C.S. Calfee, M.A. Matthay, M.D. Eisner, N. Benowitz, M. Call, J.F. Pittet, M. J. Cohen, Active and passive cigarette smoking and acute lung injury following severe blunt trauma, Am. J. Respir. Crit. Care Med. 183 (2011) 1660–1665.

[9] C.S. Calfee, M.A. Matthay, K.N. Kangelaris, E.D. Siew, D.R. Janz, G.R. Bernard, A. K. May, P. Jacob, C. Havel, N.L. Benowitz, L.B. Ware, Cigarette smoke exposure and the acute respiratory distress syndrome, Crit. Care Med. 43 (2015) 1790–1797.

[10] S. Tandon, A. Batchelor, R. Bullock, A. Gascoigne, M. Griffin, N. Hayes, J. Hing, I. Shaw, I. Warnell, S.V. Baudouin, Peri-operative risk factors for acute lung injury after elective oesophagectomy, Br. J. Anaesth. 86 (2001) 633–638.

[11] P. Wacharasint, P. Fuengfoo, N. Sukcharoen, R. Rangsin, T.-S.T. Group, Smoking increased risk of ARDS in surgical critically ill patients: results from the multicenter THAI-SICU study, Crit. Care 19 (Suppl 1) (2015), 238-238.

[12] P. Toy, O. Gajic, P. Bacchetti, M.R. Looney, M.A. Gropper, R. Hubmayr, C. A. Lowell, P.J. Norris, E.L. Murphy, R.B. Weiskopf, G. Wilson, M. Koenigsberg, D. Lee, R. Schuller, P. Wu, B. Grimes, M.J. Gandhi, J.L. Winters, D. Mair, N. Hirschler, R. Sanchez Rosen, M.A. Matthay, T.S. Group, Transfusion-related acute lung injury: incidence and risk factors, Blood 119 (2012) 1757–1767.

[13] J.M. Diamond, J.C. Lee, S.M. Kawut, R.J. Shah, A.R. Localio, S.L. Bellamy, D. J. Lederer, E. Cantu, B.A. Kohl, V.N. Lama, S.M. Bhorade, M. Crespo, E. Demissie, J. Sonett, K. Wille, J. Orens, A.S. Shah, A. Weinacker, S. Arcasoy, P.D. Shah, D. S. Wilkes, L.B. Ware, S.M. Palmer, J.D. Christie, G. Lung Transplant Outcomes, Clinical risk factors for primary graft dysfunction after lung transplantation, Am. J. Respir. Crit. Care Med. 187 (2013) 527–534.

[14] V.M. Ranieri, G.D. Rubenfeld, B.T. Thompson, N.D. Ferguson, E. Caldwell, E. Fan, L. Camporota, A.S. Slutsky, Acute respiratory distress syndrome: the Berlin Definition, JAMA 307 (2012) 2526–2533.

[15] K.M. Ho, G. Hart, D. Austin, M. Hunter, J. Botha, S. Chavan, Dose-related effect of smoking on mortality in critically ill patients: a multicentre cohort study, Intensive Care Med. 37 (2011) 981–989.

[16] S.M. Brown, E. Wilson, A.P. Presson, C. Zhang, V.D. Dinglas, T. Greene, R. O. Hopkins, D.M. Needham, with the National Institutes of Health NAN, Predictors of 6-month health utility outcomes in survivors of acute respiratory distress syndrome, Thorax 72 (2017) 311–317.

[17] K.E. Lowe, J. Zein, U. Hatipoglu, A. Attaway, Association of smoking and cumulative pack-year exposure with COVID-19 outcomes in the Cleveland clinic COVID-19 Registry, JAMA Intern. Med. 181 (5) (2021) 709–711.

[18] N.B. Johnson, L.D. Hayes, K. Brown, E.C. Hoo, K.A. Ethier, Centers for Disease Control and Prevention, CDC National Health Report: leading causes of morbidity and mortality and associated behavioral risk and protective factors–United States, 2005-2013, MMWR Suppl 63 (2014) 3–27.

[19] T. Pham, G.D. Rubenfeld, Fifty years of Research in ARDS. The epidemiology of acute respiratory distress syndrome. A 50th birthday review, Am. J. Respir. Crit. Care Med. 195 (2017) 860–870.

[20] D. Nathwani, G. Raman, K. Sulham, M. Gavaghan, V. Menon, Clinical and economic consequences of hospital-acquired resistant and multidrug-resistant Pseudomonas aeruginosa infections: a systematic review and meta-analysis, Antimicrob. Resist. Infect. Control 3 (2014) 32.

[21] F. Moazed, E.L. Burnham, R.W. Vandivier, C.M. O'Kane, M. Shyamsundar, U. Hamid, J. Abbott, D.R. Thickett, M.A. Matthay, D.F. McAuley, C.S. Calfee,

[22] Cigarette smokers have exaggerated alveolar barrier disruption in response to lipopolysaccharide inhalation, Thorax 71 (2016) 1130–1136.

[22] D. Borgas, E. Chambers, J. Newton, J. Ko, S. Rivera, S. Rounds, Q. Lu, Cigarette smoke disrupted lung endothelial barrier integrity and increased susceptibility to acute lung injury via histone deacetylase 6, Am. J. Respir. Cell Mol. Biol. 54 (2016) 683–696.

[23] Q. Lu, P. Sakhatskyy, K. Grinnell, J. Newton, M. Ortiz, Y. Wang, J. Sanchez-Esteban, E.O. Harrington, S. Rounds, Cigarette smoke causes lung vascular barrier dysfunction via oxidative stress-mediated inhibition of RhoA and focal adhesion kinase, Am. J. Physiol. Lung Cell Mol. Physiol. 301 (2011) L847–L857.

[24] P. Sakhatskyy, Z. Wang, D. Borgas, J. Lomas-Neira, Y. Chen, A. Ayala, S. Rounds, Q. Lu, Double-hit mouse model of cigarette smoke priming for acute lung injury, Am. J. Physiol. Lung Cell Mol. Physiol. 312 (2017) L56–L67.

[25] T. Strowig, J. Henao-Mejia, E. Elinav, R. Flavell, Inflammasomes in health and disease, Nature 481 (2012) 278–286.

[26] M. Lazarou, Keeping the immune system in check: a role for mitophagy, Immunol. Cell Biol. 93 (2015) 3–10.

[27] D.J. Klionsky, e al, Guidelines for the use and interpretation of assays for monitoring autophagy (3rd edition), Autophagy 12 (2016), 1-222.

[28] T.C. Stevens, C.D. Ochoa, K.A. Morrow, M.J. Robson, N. Prasain, C. Zhou, D. F. Alvarez, D.W. Frank, R. Balczon, T. Stevens, The Pseudomonas aeruginosa exoenzyme Y impairs endothelial cell proliferation and vascular repair following lung injury, Am. J. Physiol. Lung Cell Mol. Physiol. 306 (2014) L915–L924.

[29] S. McClellan, X. Jiang, R. Barrett, L.D. Hazlett, High-mobility group box 1: a novel target for treatment of Pseudomonas aeruginosa keratitis, J. Immunol. 194 (2015) 1776–1787.

[30] M. Jabaudon, R. Blondonnet, L. Roszyk, B. Pereira, R. Guerin, S. Perbet, S. Cayot, D. Bouvier, L. Blanchon, V. Sapin, J.M. Constantin, Soluble forms and ligands of the receptor for advanced glycation end-products in patients with acute respiratory distress syndrome: an observational prospective study, PLoS One 10 (2015), e0135857.

[31] T. Nakamura, E. Sato, N. Fujiwara, Y. Kawagoe, S. Maeda, S. Yamagishi, Increased levels of soluble receptor for advanced glycation end products (sRAGE) and high mobility group box 1 (HMGB1) are associated with death in patients with acute respiratory distress syndrome, Clin. Biochem. 44 (2011) 601–604.

[32] Y. Li, C.P. Gan, S. Zhang, X.K. Zhou, X.F. Li, Y.Q. Wei, J.L. Yang, M. Wu, FIP200 is involved in murine pseudomonas infection by regulating HMGB1 intracellular translocation, Cell. Physiol. Biochem. 33 (2014) 1733–1744.

[33] A.G. Drannik, M.A. Pouladi, C.S. Robbins, S.I. Goncharova, S. Kianpour, M. R. Stampfli, Impact of cigarette smoke on clearance and inflammation after Pseudomonas aeruginosa infection, Am. J. Respir. Crit. Care Med. 170 (2004) 1164–1171.

[34] J.A. Hutcherson, D.A. Scott, J. Bagaitkar, Scratching the surface - tobacco-induced bacterial biofilms, Tob. Induc. Dis. 13 (2015) 1.

[35] L. Jin, S. Batra, S. Jeyaseelan, Deletion of Nlrp3 augments survival during polymicrobial sepsis by decreasing autophagy and enhancing phagocytosis, J. Immunol. 198 (2017) 1253–1262.

[36] K.M. Robinson, K. Ramanan, M.E. Clay, K.J. McHugh, M.J. Pilewski, K. L. Nickolich, C. Corey, S. Shiva, J. Wang, R. Muzumdar, J.F. Alcorn, The inflammasome potentiates influenza/Staphylococcus aureus superinfection in mice, JCI Insight 3 (2018).

[37] K. Nakahira, J.A. Haspel, V.A. Rathinam, S.J. Lee, T. Dolinay, H.C. Lam, J. A. Englert, M. Rabinovitch, M. Cernadas, H.P. Kim, K.A. Fitzgerald, S.W. Ryter, A. M. Choi, Autophagy proteins regulate innate immune responses by inhibiting the release of mitochondrial DNA mediated by the NALP3 inflammasome, Nat. Immunol. 12 (2011) 222–230.

[38] R. Zhou, A.S. Yazdi, P. Menu, J. Tschopp, A role for mitochondria in NLRP3 inflammasome activation, Nature 469 (2011) 221–225.

[39] R.J. Youle, A.M. van der Bliek, Mitochondrial fission, fusion, and stress, Science 337 (2012) 1062–1065.

[40] P. Basilico, T.P. Cremona, A. Oevermann, A. Piersigilli, C. Benarafa, Increased myeloid cell production and lung bacterial clearance in mice exposed to cigarette smoke, Am. J. Respir. Cell Mol. Biol. 54 (2016) 424–435.

[41] P.A. Kirkham, G. Spooner, I. Rahman, A.G. Rossi, Macrophage phagocytosis of apoptotic neutrophils is compromised by matrix proteins modified by cigarette smoke and lipid peroxidation products, Biochem. Biophys. Res. Commun. 318 (2004) 32–37.

[42] J.C. Phipps, D.M. Aronoff, J.L. Curtis, D. Goel, E. O'Brien, P. Mancuso, Cigarette smoke exposure impairs pulmonary bacterial clearance and alveolar macrophage complement-mediated phagocytosis of Streptococcus pneumoniae, Infect. Immun. 78 (2010) 1214–1220.

[43] H.H. Dar, Y.Y. Tyurina, K. Mikulska-Ruminska, I. Shrivastava, H.C. Ting, V. A. Tyurin, J. Krieger, C.M. St Croix, S. Watkins, E. Bayir, G. Mao, C.R. Armbruster, A. Kapralov, H. Wang, M.R. Parsek, T.S. Anthonymuthu, A.F. Ogunsola, B. A. Flitter, C.J. Freedman, J.R. Gaston, T.R. Holman, J.M. Pilewski, J. S. Greenberger, R.K. Mallampalli, Y. Doi, J.S. Lee, I. Bahar, J.M. Bomberger, H. Bayir, V.E. Kagan, Pseudomonas aeruginosa utilizes host polyunsaturated phosphatidylethanolamines to trigger theft-ferroptosis in bronchial epithelium, J. Clin. Invest. 128 (2018) 4639–4653.

[44] E. Morello, T. Perez-Berezo, C. Boisseau, T. Baranek, A. Guillon, D. Brea, P. Lanotte, X. Carpena, N. Pietrancosta, V. Herve, R. Ramphal, N. Cenac, M. Si-Tahar, Pseudomonas aeruginosa lipoxygenase LoxA contributes to lung infection by altering the host immune lipid signaling, Front. Microbiol. 10 (2019) 1826.

[45] J. Ousingsawat, R. Schreiber, E. Gulbins, M. Kamler, K.P. Kunzelmann, Aeruginosa induced lipid peroxidation causes ferroptotic cell death in airways, Cell. Physiol. Biochem. 55 (2021) 590–604.

[46] E.D. Chambers, A. White, A. Vang, Z. Wang, A. Ayala, T. Weng, M. Blackburn, G. Choudhary, S. Rounds, Q. Lu, Blockade of equilibrative nucleoside transporter 1/2 protects against Pseudomonas aeruginosa-induced acute lung injury and NLRP3 inflammasome activation, Faseb. J. 34 (2020) 1516–1531.

[47] M.J. Schultz, A.W. Rijneveld, S. Florquin, C.K. Edwards, C.A. Dinarello, T. van der Poll, Role of interleukin-1 in the pulmonary immune response during Pseudomonas aeruginosa pneumonia, Am. J. Physiol. Lung Cell Mol. Physiol. 282 (2002) L285–L290.

[48] M.J. Schultz, S. Knapp, S. Florquin, J. Pater, K. Takeda, S. Akira, T. van der Poll, Interleukin-18 impairs the pulmonary host response to Pseudomonas aeruginosa, Infect. Immun. 71 (2003) 1630–1634.

[49] R. Costeira, K.A. Lee, B. Murray, C. Christiansen, J. Castillo-Fernandez, M. Ni Lochlainn, J. Capdevila Pujol, H. Macfarlane, L.C. Kenny, I. Buchan, J. Wolf, J. Rymer, S. Ourselin, C.J. Steves, T.D. Spector, L.R. Newson, J.T. Bell, Estrogen and COVID-19 symptoms: associations in women from the COVID symptom study, PLoS One 16 (2021), e0257051.

[50] Z. Yang, Y.C. Huang, H. Koziel, R. de Crom, H. Ruetten, P. Wohlfart, R. W. Thomsen, J.A. Kahlert, H.T. Sorensen, S. Jozefowski, A. Colby, L. Kobzik, Female resistance to pneumonia identifies lung macrophage nitric oxide synthase-3 as a therapeutic target, Elife 3 (2014).

[51] R.A. Porritt, J.L. Markman, D. Maruyama, B. Kocaturk, S. Chen, T.J.A. Lehman, Y. Lee, M.C. Fishbein, M. Noval Rivas, M. Arditi, Interleukin-1 beta-mediated sex differences in Kawasaki disease vasculitis development and response to treatment, Arterioscler. Thromb. Vasc. Biol. 40 (2020) 802–818.

[52] H. Bessler, M. Osovsky, B. Beilin, Y. Alcalay, L. Sirota, The existence of gender difference in IL-1Ra gene polymorphism, J. Interferon Cytokine Res. 27 (2007) 931–935.

[53] N. Reiniger, M.M. Lee, F.T. Coleman, C. Ray, D.E. Golan, G.B. Pier, Resistance to Pseudomonas aeruginosa chronic lung infection requires cystic fibrosis transmembrane conductance regulator-modulated interleukin-1 (IL-1) release and signaling through the IL-1 receptor, Infect. Immun. 75 (2007) 1598–1608.

[54] C.J. Fisher Jr., J.F. Dhainaut, S.M. Opal, J.P. Pribble, R.A. Balk, G.J. Slotman, T. J. Iberti, E.C. Rackow, M.J. Shapiro, R.L. Greenman, et al., Recombinant human interleukin 1 receptor antagonist in the treatment of patients with sepsis syndrome. Results from a randomized, double-blind, placebo-controlled trial. Phase III rhIL-1ra Sepsis Syndrome Study Group, JAMA 271 (1994) 1836–1843.

[55] S.M. Opal, C.J. Fisher Jr., J.F. Dhainaut, J.L. Vincent, R. Brase, S.F. Lowry, J. C. Sadoff, G.J. Slotman, H. Levy, R.A. Balk, M.P. Shelly, J.P. Pribble, J. F. LaBrecque, J. Lookabaugh, H. Donovan, H. Dubin, R. Baughman, J. Norman, E. DeMaria, K. Matzel, E. Abraham, M. Seneff, Confirmatory interleukin-1 receptor antagonist trial in severe sepsis: a phase III, randomized, double-blind, placebo-controlled, multicenter trial. The Interleukin-1 Receptor Antagonist Sepsis Investigator Group, Crit. Care Med. 25 (1997) 1115–1124.

[56] M.T. Ganter, J. Roux, B. Miyazawa, M. Howard, J.A. Frank, G. Su, D. Sheppard, S. M. Violette, P.H. Weinreb, G.S. Horan, M.A. Matthay, J.F. Pittet, Interleukin-1beta causes acute lung injury via alphavbeta5 and alphavbeta6 integrin-dependent mechanisms, Circ. Res. 102 (2008) 804–812.

[57] M. Tamaru, K. Tomura, S. Sakamoto, K. Tezuka, T. Tamatani, S. Narumi, Interleukin-1beta induces tissue- and cell type-specific expression of adhesion molecules in vivo, Arterioscler. Thromb. Vasc. Biol. 18 (1998) 1292–1303.

[58] J. Sun, J. Chen, J. Cao, T. Li, S. Zhuang, X. Jiang, IL-1beta-stimulated beta-catenin up-regulation promotes angiogenesis in human lung-derived mesenchymal stromal cells through a NF-kappaB-dependent microRNA-433 induction, Oncotarget 7 (2016) 59429–59440.

[59] V. Kirkin, History of the selective autophagy Research: how did it begin and where does it stand today? J. Mol. Biol. 432 (2020) 3–27.

[60] B. Zou, J. Liu, D.J. Klionsky, D. Tang, R. Kang, Extracellular SQSTM1 as an inflammatory mediator, Autophagy 16 (2020) 2313–2315.

[61] H.M. Lee, J.M. Yuk, K.H. Kim, J. Jang, G. Kang, J.B. Park, J.W. Son, E.K. Jo, Mycobacterium abscessus activates the NLRP3 inflammasome via Dectin-1-Syk and p62/SQSTM1, Immunol. Cell Biol. 90 (2012) 601–610.